

Epidemiology-informed Graph Neural Network for Heterogeneity-aware Epidemic Forecasting

Yufan Zheng
City University of Hong Kong
Hong Kong, China
zhipre@gmail.com

Wei Jiang
The University of Queensland
Brisbane, Australia
wei.jiang@uq.edu.au

Alexander Zhou
The Hong Kong Polytechnic University
Hong Kong, China
alexander.zhou@polyu.edu.hk

Nguyen Quoc Viet Hung
Griffith University
Brisbane, Australia
henry.nguyen@griffith.edu.au

Choujun Zhan
South China Normal University
Guangzhou, China
zchoujun2@gmail.com

Tong Chen*
The University of Queensland
Brisbane, Australia
tong.chen@uq.edu.au

Abstract—Among various spatio-temporal prediction tasks, epidemic forecasting plays a critical role in public health management. Recent studies have demonstrated the strong potential of spatio-temporal graph neural networks (STGNNs) in extracting heterogeneous spatio-temporal patterns for epidemic forecasting. However, most of these methods bear an over-simplified assumption that two locations (e.g., cities) with similar observed features in previous time steps will develop similar infection numbers in the future. In fact, for any epidemic disease, there exists strong heterogeneity of its intrinsic evolution mechanisms across geolocation and time, which can eventually lead to diverged infection numbers in two “similar” locations. However, such mechanistic heterogeneity is non-trivial to be captured due to the existence of numerous influencing factors like medical resource accessibility, virus mutations, mobility patterns, etc., most of which are spatio-temporal yet unreachable or even unobservable. To address this challenge, we propose a Heterogeneous Epidemic-Aware Transmission Graph Neural Network (HeatGNN), a novel epidemic forecasting framework. By binding the epidemiology mechanistic model into a GNN, HeatGNN learns epidemiology-informed location embeddings of different locations that reflect their own transmission mechanisms over time. With the time-varying mechanistic affinity graphs computed with the epidemiology-informed location embeddings, a heterogeneous transmission graph network is designed to encode the mechanistic heterogeneity among locations, providing additional predictive signals to facilitate accurate forecasting. Experiments on three benchmark datasets have revealed that HeatGNN outperforms various strong baselines. Moreover, our efficiency analysis verifies the real-world practicality of HeatGNN on datasets of different sizes.

Index Terms—Spatio-temporal Graphs, Predictive Analytics, Epidemic Forecasting

I. INTRODUCTION

The outbreak and spread of epidemics are massive disasters facing global human society, which can cause a substantial number of deaths or irreversible physiological damage to humans [1] as well as significant economic losses across various industries worldwide [2]. Recent global outbreaks, such as COVID-19, have placed unprecedented pressure on public

health systems and decision-makers [3]. In response, there has been a growing interest in developing accurate and effective epidemic forecasting models [4], [5]. These models can support the implementation of public health interventions [6], optimize resource allocation [7], and enhance public awareness of early prevention and control strategies [8], thereby helping to prevent and control the onset and rapid spread of epidemics.

In a nutshell, epidemic forecasting predicts the infection numbers at geographically connected regions in the future horizon based on existing records. Traditional epidemic models, like the Susceptible-Infected-Recovered (SIR) model, rely on mechanistic approaches and location networks to simulate multi-regional transmission for epidemic forecasting [9]–[11]. Despite advantageous explainability and applicability, these models exhibit limited capacity to capture real-world complexities. As such, with the rapid development of machine learning, methods represented by spatio-temporal graph neural networks (STGNNs) have been used to learn spatial and temporal dependencies in epidemic transmission simultaneously [4], [5], [12]–[16]. However, many STGNNs are purely data-driven methods that neglect the underlying epidemic transmission mechanisms, making them prone to overfitting historical data and being misled by spurious features. To address the limitations of both sides, epidemiological machine learning (EML) models [17]–[19] have been proposed by incorporating mechanistic laws into a machine learning backbone to enhance the model’s generalizability and robustness. This trend also extends to STGNNs, where the time- and location-sensitive parameters in epidemic models are predicted to support dynamic epidemic forecasting [20], [21].

Generally, a key to epidemic forecasting is heterogeneity discovery, such that similar spatio-temporal patterns among locations can be aligned to enhance predictions while dissimilar ones are filtered out. This also explains the popularity of STGNNs for this task owing to their capability of learning the semantic affinity of connected locations within the topology of the graph. Meanwhile, existing models commonly use an over-simplified assumption that such heterogeneity only

* Corresponding author.

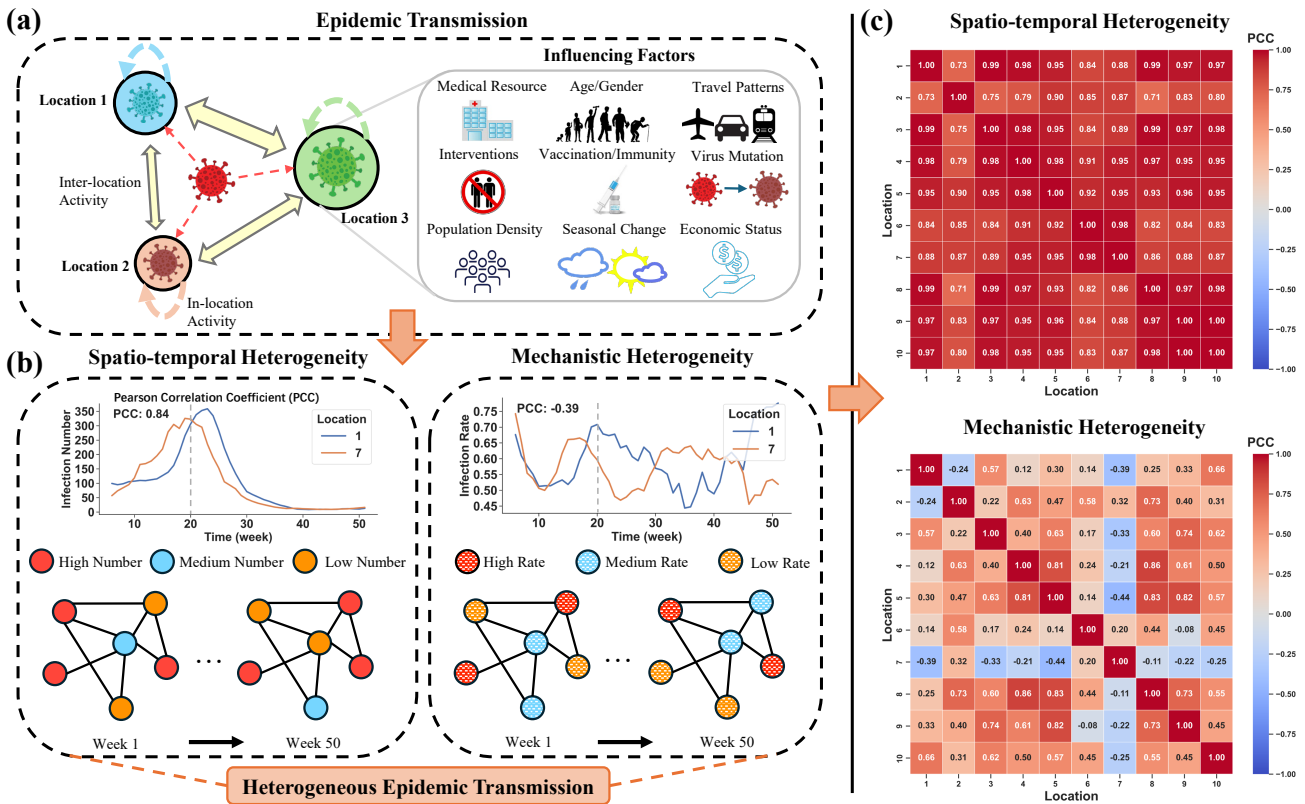


Fig. 1: Spatio-temporal and mechanistic heterogeneity between different locations in epidemic transmission. (a) Epidemic transmission with different influencing factors. (b) Example of heterogeneous epidemic transmission between two locations. (c) The analyses of two heterogeneities on a real-world dataset (US-Regions).

exists within observed features, such as past infection number, population, and demographic statistics of a region. However, in reality, epidemic heterogeneity holds for not only spatio-temporal features, but also the underlying intrinsic epidemic transmission mechanism. In this paper, we refer to these two types of heterogeneity as *spatio-temporal heterogeneity* and *mechanistic heterogeneity*, respectively. For illustration, we provide an example in Figure 1. In a nutshell, while spatio-temporal heterogeneity compares observed features (i.e., what they are now), like infection numbers, the mechanistic heterogeneity highlights the evolutionary trajectories of each location (i.e., how they will change), such as infection rates. It is worth noting that the two heterogeneity types are not mutually substitutable but rather complementary. For instance, though the two locations in Figure 1(b) have similar patterns in their infection numbers until the 20th week, the numbers have moved toward different directions in the following two weeks because of the distinct dynamics in the two locations' infection rates. In the real epidemic transmission process, the two heterogeneity signals can vary greatly, as depicted by the Pearson Correlation Coefficient (PCC) across locations from a sampled time step (Figure 1(c)). Hence, if only the spatio-temporal heterogeneity is considered in the STGNN, the model is prone to making inaccurate predictions in the long term.

To this end, bringing awareness of the mechanistic hetero-

geneity to the prediction model appears to be a beneficial move. However, learning such heterogeneity incurs non-trivial challenges. The first challenge lies in effectively understanding and mimicking the underlying intrinsic transmission mechanisms, which are jointly determined by a complex suite of factors. As shown in Figure 1(a), those influencing factors [6], [8], [22]–[26] include (but are not limited to) public health resources, policy interventions, climates, individual or group susceptibility, virus mutations, and so on, many of which are not linked to the epidemic records and are even unobservable. Consequently, this renders explicit and precise modeling of the intrinsic epidemic transmission mechanism infeasible. At the same time, the second challenge is the modeling of the similarity/dissimilarity across the epidemic transmission mechanism of distinct regions. The root cause is the lack of effective measures to represent and quantify the mechanistic heterogeneity across locations, preventing it from providing more predictive signals into epidemic forecasting.

To address these challenges, we propose an innovative framework for heterogeneous epidemic transmission forecasting modeling: **Heterogeneous Epidemic-Aware Transmission Graph Neural Network (HeatGNN)**. This framework aims to improve epidemic forecasting performance by simultaneously learning spatio-temporal and mechanistic heterogeneity. Firstly, we introduce epidemiology-informed embedding learn-

ing to encapsulate the mechanistic patterns into each location’s representation. To bypass the intricacy and unavailability of all possible influencing factors, instead of simulating the explicit mechanistic process of epidemic transmission, we parameterize the time-varying SIR model for each location with its spatio-temporal graph embedding. By aligning the behaviors of the implicitly parameterized time-varying SIR model and the explicitly derived one, the epidemiology-informed embedding can be effectively optimized. Secondly, to quantify and take full advantage of the mechanistic heterogeneity across locations, we propose to learn the time-varying mechanistic affinity graphs. Each mechanistic affinity graph is constructed based on the pairwise similarity between two epidemiology-informed location embeddings, where a sparsification approach is in place to remove noisy connections and ensure efficiency. With a backbone STGNN, the spatio-temporal and mechanistic heterogeneities are captured by respectively modeling the geographical and mechanistic affinity graphs across time steps to facilitate heterogeneity-aware epidemic forecasting. In summary, our main contributions are as follows:

- In the context of epidemic forecasting, we characterize two types of heterogeneity, namely, spatio-temporal heterogeneity and mechanistic heterogeneity. We point out that on top of the commonly used spatio-temporal heterogeneity, mechanistic heterogeneity is a largely overlooked yet crucial predictive signal for predicting future infection numbers.
- We propose HeatGNN, a novel framework for heterogeneous epidemic forecasting that jointly discovers spatio-temporal and mechanistic heterogeneity. By incorporating a well-defined mechanistic model into the STGNN, HeatGNN learns epidemiology-informed location embedding and mechanistic affinity graphs to account for mechanistic heterogeneity across locations to greatly benefit the predictive performance.
- Our framework achieves state-of-the-art performance across three real-world epidemic datasets. Our efficiency analysis demonstrates that HeatGNN’s inference time is highly scalable w.r.t. the number of locations involved in the task.

II. PRELIMINARY

A. Problem Formalization

In epidemic transmission, we formulate the epidemic forecasting problem as a node-level regression task on graphs. There are N locations of interest in an area; each location (e.g., a region, city, or state) is represented as a node. Given the spatio-temporal observations of epidemic transmission risk dynamics: $\mathbf{X} = \{\mathbf{x}_1, \mathbf{x}_2, \dots, \mathbf{x}_T\}^T \in \mathbb{R}^{T \times N}$, where T represents the length of time step (e.g., the infected population number or infection number for T weeks). Each $\mathbf{x}_t = \{x_{t,1}, x_{t,2}, \dots, x_{t,N}\} \in \mathbb{R}^{N \times 1} (t = 1, 2, \dots, T)$ is an N -dimensional vector, with $x_{t,i} (i = 1, 2, \dots, N)$ being the epidemic transmission risk at the time step t in the location i . The epidemic is transmitted in different areas, let $\mathcal{G} = (\mathcal{V}, \mathcal{E})$

be a geographical graph, where \mathcal{V} is the nodes set comprising $|\mathcal{V}| = N$ nodes (e.g., regions, cities, or states). The $\mathcal{E} \subseteq \mathcal{V} \times \mathcal{V}$ is the geographic link between these nodes. The adjacency matrix $\mathcal{A} \in \mathbb{R}^{N \times N}$ of the geographical graph is formulated as $\mathcal{A}_{ij} = 1$ if there is an edge $e_{ij} \in \mathcal{E}$, and $\mathcal{A}_{ij} = 0$ otherwise.

The objective of this work is to accurately predict the infection number in each location. Given the historical data and the adjacency matrix of the geographical graph, we can develop a predictive model f , which can be formulated as follows:

$$\mathbf{x}_{t+h} = f(\mathbf{X}_{t-w+1:t}, \mathcal{A}), \quad (1)$$

where \mathbf{x}_{t+h} is an epidemic transmission risk in a future time step $t+h$ and h represents the forecasting horizon (e.g., the number of time steps to be predicted ahead). $\mathbf{X}_{t-w+1:t} = \{\mathbf{x}_{t-w+1}, \mathbf{x}_{t-w+2}, \dots, \mathbf{x}_t\} \in \mathbb{R}^{w \times N}$ is the historical epidemic transmission risk, w represents the window size of historical input, and N is number of locations.

III. METHODOLOGIES

The proposed framework, as shown in Figure 2, consists of four modules: 1) Spatio-temporal Graph Learning (STGL) Module; 2) Epidemiology-informed Embedding Learning (EIEL) Module; 3) Transmission Graph (TG) Module; and 4) Epidemic Forecasting Decoder Module. In the following subsections, we describe each module in more detail.

A. Spatio-temporal Graph Learning Module

The spread of an epidemic in a city is influenced by nearby cities with similar geographic features, as adjacent locations have similar weather and topographical conditions, leading to comparable epidemic transmission patterns. Conversely, distinct weather and topography can result in varying patterns of spread. These differences lead to the emergence of spatio-temporal heterogeneity in epidemic transmission. To capture spatio-temporal heterogeneity, we propose using the STGL module in epidemic forecasting. The STGL module utilizes historical data to learn dynamic time series variations and geographic interactions, enabling it to capture the spatio-temporal heterogeneity of epidemic transmission across locations. EpiGNN is a graph neural network-based epidemic forecasting model that considers local and global spatial effects of regions and captures spatio-temporal dependencies well in some datasets [12]. Therefore, we use the backbone of EpiGNN as our STGL module. Given the historical epidemic transmission risk $\mathbf{X}_{t-w:t}$ and the adjacency matrix \mathcal{A} of geographic topology, the spatio-temporal (ST) embedding $\mathbf{P}_t \in \mathbb{R}^{N \times D_1}$ with D_1 -dimensional containing spatio-temporal heterogeneity information in N locations can be described as:

$$\mathbf{P}_t = f_{\text{ST}}(\mathcal{A}, \mathbf{X}_{t-w:t}), \quad (2)$$

where f_{ST} is the STGL module.

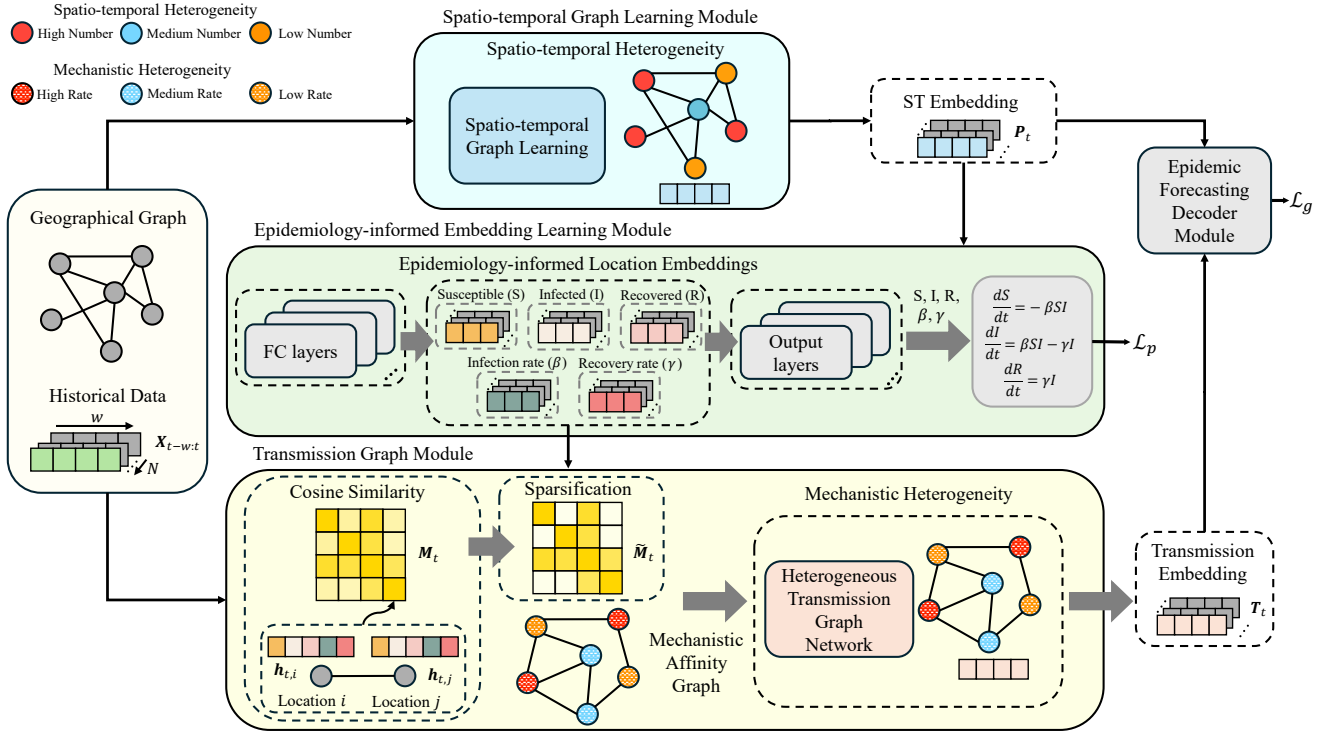


Fig. 2: The schematic illustration of HeatGNN.

B. Epidemiology-informed Embedding Learning Module

The STGL module only captures the spatio-temporal heterogeneity among different locations, while many previous approaches predict epidemic transmission directly based on the learned ST embedding. However, only capturing the spatio-temporal pattern of the infected population is noisy for epidemic forecasting and lacks the intrinsic epidemic transmission mechanism, which is prone to producing generalization errors in predictions [18]. Therefore, we use the epidemiology mechanistic model to enhance the process of learning location transmission dynamics to capture latent patterns and reflect well-defined disease dissemination mechanisms. Given a location i , we assign the time-varying SIR model as the epidemiology mechanistic model, which can be described as following ordinary differential equations (ODEs):

$$\begin{cases} \frac{dS_i}{dt} = -\beta_i S_i I_i, \\ \frac{dI_i}{dt} = \beta_i S_i I_i - \gamma_i I_i, \\ \frac{dR_i}{dt} = \gamma_i I_i, \end{cases} \quad (3)$$

where S_i , I_i , and R_i represent the number of susceptible, infected, and recovered populations in location i , respectively. β_i and γ_i are the time-dependent parameters, which mean the infection rate of susceptible populations and the recovery rate of infected populations in the location i . Here, we follow the assumption that the total population $N_i = S_i + I_i + R_i$ consists of susceptible, infected, and recovered populations.

Although the time-varying SIR model reflects the intrinsic epidemic transmission mechanism, it requires high computational costs and domain knowledge to predict its large-scale parameters simultaneously. In addition, the variables of the time-varying SIR model are heavily entangled, and it is difficult to focus only on predicting changes in the number of infected populations (I) in epidemic forecasting. These challenges motivate us to propose the EIEL module that uses node embeddings to parameterize the five time-varying SIR variables. The EIEL module uses five different multi-layer perceptrons (MLPs) to predict susceptible S , infected I , recovered R , infection rate β , and recovery rate γ in the time-varying SIR model at each location and time step. Each MLP consists of a fully connected (FC) layer with L layers and an output layer. Additionally, to enhance the embedding capacity of the EIEL module, we learn epidemiology-informed location embeddings based on the ST embedding $P_t = \{p_{t,1}, p_{t,2}, \dots, p_{t,N}\} \in \mathbb{R}^{N \times D_1}$. Then, based on i -th location ST embedding $p_{t,i} \in \mathbb{R}^{D_1}$, the epidemiology-informed location embedding $e_{j,i} \in \mathbb{R}^{D_2}$ of j -th time-varying SIR variable in i -th location can be computed by the j -th FC layer with L layers:

$$e_{j,i} = g_j \left(p_{t,i}; \{W_j^{(l)}, b_j^{(l)}, \sigma_j^{(l)}\}_{l=1}^L \right), \quad (4)$$

where $W_j^{(l)}$ is the weight matrix of the l -th hidden layer of the j -th FC layer, $b_j^{(l)}$ is its bias vector, and $\sigma_j^{(l)}$ is the activation function. Through five FC layers, we obtain the epidemiology-informed location embeddings $h_{t+h,i} =$

$[e_{1,i}; e_{2,i}; e_{3,i}; e_{4,i}; e_{5,i}] \in \mathcal{R}^{5D_2}$ for i -th location in time step $t+h$. To predict the dynamic epidemic transmission, the output of MLP is defined as follows:

$$y_{j,i} = \sigma_j^{(2)}(\mathbf{W}_j^{(2)} e_{j,i} + \mathbf{b}_j^{(2)}), \quad (5)$$

where $y_{j,i} \in \{\hat{S}_{t+h,i}, \hat{I}_{t+h,i}, \hat{R}_{t+h,i}, \hat{\beta}_{t+h,i}, \hat{\gamma}_{t+h,i}\}$ one of five variables of the susceptible S , infected I , recovered R , infection rate β , and recovery rate γ at location i at time step $t+h$. $\mathbf{W}_j^{(2)}$, $\mathbf{b}_j^{(2)}$, and $\sigma_j^{(2)}$ are the weight matrix, bias vector, and activation function in the output layer of the j -th MLP, respectively. In Section III-E, we introduce the optimization of the EIEL module to ensure that the learned epidemiology-informed location embedding is consistent with the intrinsic epidemic transmission mechanism.

C. Transmission Graph Module

1) *Mechanistic Affinity Graph*: The EIEL captures the intrinsic epidemic transmission mechanism of each location separately but cannot learn the interactive relationships between them. To further capture the differences in intrinsic epidemic transmission mechanisms between locations, we propose a time-varying mechanistic affinity graph (MAG) that can efficiently characterize the mechanistic heterogeneity between locations. The MAG $\widetilde{\mathbf{M}}_t \in \mathbb{R}^{N \times N}$ is calculated by the cosine similarity function ϕ between the epidemiology-informed location embeddings of different locations. The mechanistic similarity between locations is defined as follows:

$$m_{ij} = \phi(\mathbf{h}_{t,i}, \mathbf{h}_{t,j}), \quad (6)$$

where the mechanistic similarity $m_{ij} \in \mathbf{M}_t$ represent the mechanistic dependence between i -th location and j -th location based on epidemiology-informed location embeddings ($\mathbf{h}_{t,i}$ and $\mathbf{h}_{t,j}$) of two locations at time step t . \mathbf{M}_t is a symmetric matrix. Then, we normalize the similarity between different locations:

$$\widetilde{\mathbf{M}}_t = \mathbf{D}^{-\frac{1}{2}} \mathbf{M}_t \mathbf{D}^{-\frac{1}{2}}, \quad (7)$$

where \mathbf{D} is degree matrix of \mathbf{M}_t . To focus on the key mechanistic dependence, reduce redundant information, and enhance the computational efficiency of GNNs, we design an indicator function to sparsify the MAG $\widetilde{\mathbf{M}}_t \in [0, 1]$. This sparsification is controlled by a sparse threshold δ , applied to each normalized similarity $\tilde{m}_{ij} \in \widetilde{\mathbf{M}}_t$:

$$\tilde{m}_{ij} = \begin{cases} \tilde{m}_{ij} & \text{if } \tilde{m}_{ij} \geq \delta \\ 0 & \text{otherwise.} \end{cases}, \quad (8)$$

2) *Heterogeneous Transmission Graph Network*: To fully capture the complex mechanistic heterogeneity by utilizing the mechanistic dependence in the MAG, we propose the Heterogeneous Transmission Graph Network (HTGN) to encode the transmission embedding between locations. The HTGN integrates a MAG with the architecture of Spatio-Temporal Graph Convolutional Networks (STGCN) [27], which comprises two spatio-temporal convolutional blocks (ST-blocks). Given that the historical epidemic transmission risk $\mathbf{X}_{t-w+1:t}$

and a MAG $\widetilde{\mathbf{M}}_t$ in time step t , we learn the transmission embedding $\mathbf{T}_t \in \mathbb{R}^{N \times D_3}$ of mechanistic heterogeneity by ST-Blocks:

$$\mathbf{T}_t = \text{ST-Blocks}(\widetilde{\mathbf{M}}_t, \mathbf{X}_{t-w+1:t}), \quad (9)$$

D. Epidemic Forecasting Decoder Module

Finally, by simultaneously capturing the spatio-temporal heterogeneity and mechanistic heterogeneity across different locations, our framework applies an FC layer to predict future epidemic transmission risk, providing the epidemic forecasting result $\hat{\mathbf{Y}}_{t+h}$ in time step $t+h$:

$$\hat{\mathbf{Y}}_{t+h} = \mathbf{W}[\mathbf{P}_t; \mathbf{T}_t] + \mathbf{b}, \quad (10)$$

where \mathbf{W} and \mathbf{b} are the weight matrix and basis vector, respectively, \mathbf{P}_t is the ST embedding learned from the STGL module and \mathbf{T}_t is the transmission embedding learned from the G module.

E. Optimization

To ensure the epidemiology-informed location embeddings are consistent with the mechanism of the intrinsic epidemic transmission, we use the idea from the PINN [28] to propose a physics loss to inform the learning process in the EIEL module. The physics loss incorporates the underlying physical laws of the intrinsic epidemic transmission mechanism into the EIEL module. Specifically, we aim to solve the time-varying SIR model using five MLPs by minimizing the multi-objective physics loss \mathcal{L}_p . Given the prediction of five variables ($\hat{S}_{t+h,i}$, $\hat{I}_{t+h,i}$, $\hat{R}_{t+h,i}$, $\hat{\beta}_{t+h,i}$, and $\hat{\gamma}_{t+h,i}$) of time-varying SIR model, the physics loss \mathcal{L}_p to be described as follows:

$$\begin{aligned} \mathcal{L}_d(\hat{I}_{t+h,i}) &= \frac{1}{N} \sum_{i=1}^N |\hat{I}_{t+h,i} - x_{t+h,i}|, \\ \mathcal{L}_o(\hat{S}_{t+h,i}, \hat{I}_{t+h,i}, \hat{\beta}_{t+h,i}, \hat{\gamma}_{t+h,i}) &= \frac{1}{N} \sum_{i=1}^N \left| \frac{d\hat{I}_{t+h,i}}{d} - (\hat{\beta}_{t+h,i} \hat{S}_{t+h,i} \hat{I}_{t+h,i} - \hat{\gamma}_{t+h,i} \hat{I}_{t+h,i}) \right|, \\ \mathcal{L}_p &= \mathcal{L}_d(\hat{I}_{t+h,i}) + \mathcal{L}_o(\hat{S}_{t+h,i}, \hat{I}_{t+h,i}, \hat{\beta}_{t+h,i}, \hat{\gamma}_{t+h,i}), \end{aligned} \quad (11)$$

where $x_{t+h,i}$ is the ground truth. \mathcal{L}_d represents the error between predicted values and ground truth, which uses mean absolute error (MAE) as a loss measure. \mathcal{L}_o is the residual term of the ODEs set. We use \mathcal{L}_d to constrain the output of MLPs consistent with the real-world epidemic transmission dynamics and use \mathcal{L}_o to constrain the output consistent with the mechanism of intrinsic epidemic transmission.

In our framework, we use the forecasting from the epidemic forecasting decoder module as the final forecasting result and use the MAE loss to compare it with the ground truth.

$$\mathcal{L}_g = \frac{1}{N} \sum_{i=1}^N |\hat{y}_{t+h,i} - x_{t+h,i}|, \quad (12)$$

where $\hat{y}_{t+h,i} \in \hat{\mathbf{Y}}_{t+h}$ is output value of HeatGNN and $x_{t+h,i}$ is the ground truth value. Finally, the main objective function \mathcal{L} of HeatGNN is given as follows:

$$\mathcal{L} = \mathcal{L}_g + \lambda \mathcal{L}_p, \quad (13)$$

where the loss term \mathcal{L}_g is forecasting the error of our proposed framework and minimizing it to achieve good performance. Another loss term \mathcal{L}_p is used as a regularizer of the EIEL module to enhance the ability of this module to represent the intrinsic epidemic transmission mechanism. The loss weight λ is used to balance two different loss terms.

IV. EXPERIMENTS

In the experiment, we evaluate our proposed framework HeatGNN by answering the below research questions (RQs):

- **RQ1:** Does HeatGNN outperform the existing state-of-the-art epidemic forecasting models?
- **RQ2:** What is the impact of each core component in HeatGNN?
- **RQ3:** What is the performance of HeatGNN with different hyperparameters?
- **RQ4:** Is HeatGNN reliable for short-term and long-term epidemic forecasting?
- **RQ5:** Does HeatGNN have robust scalability?

A. Datasets

We evaluate the performance of our framework using three real-world datasets following previous work [4]: Japan-Prefectures, US-States, and US-Regions.

- **Japan-Prefectures:** This dataset comprises weekly influenza-like-illness levels from August 2012 to March 2019 for 47 prefectures in Japan collected from the Weekly Infectious Diseases Report in Japan.
- **US-Regions:** This dataset includes weekly influenza activity levels (flu patient counts) from 2002 to 2017 for 10 Health and Human Services regions in the United States collected from the Department of Health and Human Services.
- **US-States:** This dataset contains weekly influenza disease data (positive cases) from 2010 to 2017 for 49 states in the United States collected from the Center for Disease Control.

The statistics of these three datasets are summarized in Table I. The US-Regions dataset has a higher mean and greater data volatility, the US-States dataset has a lower mean and more concentrated data distribution, and the Japan-Prefectures dataset is between the other two regarding numerical range and data dispersion.

TABLE I: Statistics of the three real-world datasets.

Dataset	Size	Min	Max	Mean	SD
Japan-Prefectures	47 × 348	0	26635	655	1711
US-Regions	10 × 785	0	16526	1009	1351
US-States	49 × 360	0	9716	223	428

B. Evaluation Metrics

The Root Mean Squared Error (RMSE) measures the difference between predicted and ground truth values after projecting the normalized values into the real range:

$$\text{RMSE} = \sqrt{\frac{1}{N} \sum_{i=1}^N (\hat{y}_i - y_i)^2}, \quad (14)$$

The PCC is a measure of the linear dependence between two sets of values:

$$\text{PCC} = \frac{\sum_{i=1}^N (\hat{y}_i - \bar{\hat{y}})(y_i - \bar{y})}{\sqrt{\sum_{i=1}^N (\hat{y}_i - \bar{\hat{y}})^2} \sqrt{\sum_{i=1}^N (y_i - \bar{y})^2}}, \quad (15)$$

where \hat{y} is the predicted values, y is the ground truth values, and $\bar{\hat{y}}$ and \bar{y} are their average values respectively. N represents the number of samples.

C. Experimental Settings and Implementation Details

We divide the dataset into training, validation, and test sets in chronological order with a ratio of 60%-20%-20% [20], [29]. We normalized all data based on the training data. The validation set is used for hyperparameter tuning and to prevent overfitting. The test set is used to evaluate the performance of the final model using RMSE and PCC [29]. The smaller the RMSE, the better the performance while the larger the PCC, the better the performance. We used Adam [30] as the optimizer with weight decay 5e-4 during training. The grid search is used to find the best hyperparameter combinations. After the grid search, we set the initial learning rate to 0.001, the early stopping strategy with the patience of 200 epochs, the batch size to 32, and the number of epochs to 1500. All the parameters are initialized using Xavier initialization in HeatGNN. For all models, we set the historical window size w to 20, that is, to use the historical data of the previous 20 weeks as input features. The horizon of advance forecasting h is 2, 3, 4, and 5, that is, to predict the risk of epidemic transmission of the h -th week after time step t . All experimental results are the average of 5 randomized trials. The experiments are conducted on an Intel Xeon Silver 4214 Processor CPU with 128 GB of 2666 MHz RAM and 4 NVIDIA TITAN RTX 24GB GPUs. Our method implemented in Python 3.8 and PyTorch 1.13.1 trains on GPUs in 30-60 minutes for each forecasting task.

D. Comparison Methods

We compared four types of models: traditional statistical models, RNN-based and CNN-based models, STGNN models, and EML models. The traditional statistical models include AutoRegressive (AR), AutoRegressive Moving Average (ARMA), Generalized AutoRegressive (GAR), and Vector AutoRegression (VAR). The RNN-based and CNN-based models include Recurrent Neural Network (RNN) [31], Long Short-Term Memory (LSTM) [32], Gated Recurrent Unit (GRU) [33], RNN-Attn [34], CNNRNN-Res [29], and Long- and Short-term Time-series Network (LSTNet) [35]. The STGNN models include STGCN [27], Multiresolution

Graph Neural Networks (MGNN) [15], Temporal Multiresolution Graph Neural Networks (TMGNN) [15], Attention-based Multiresolution Graph Neural Networks (ATMGNN) [16], Cross-location Attention-based Graph Neural Networks (Cola-GNN) [4], and Epi-GNN [12]. The EML model is Epi-Cola-GNN [20].

E. Overall Comparison

This section addresses **RQ1**. We evaluate our method in both short-term forecasting (horizon=2, 3) and long-term forecasting (horizon=4, 5) settings. We exclude the case of horizon=1 due to delays in epidemic surveillance data, as extreme short-term forecasting does not provide sufficient time for effective interventions. Table II summarizes the results of all methods under three real-world datasets. While the PCC shows relatively stable ranges and variances between datasets, the RMSE shows significant variability, primarily driven by differences in the variance of the datasets.

Compared with various baseline models, including traditional statistical, RNN-based, CNN-based, STGNN, and EML models, HeatGNN achieves the lowest RMSE and highest PCC across most horizons and datasets. These results demonstrate its capability to capture both spatio-temporal heterogeneity and mechanistic heterogeneity effectively. The high PCC values across datasets and horizons highlight the robustness of HeatGNN in capturing transmission patterns that are closely related to real-world data, making it well-suited for short-term and long-term epidemic forecasting. For instance, in the Japan-Prefectures dataset, HeatGNN achieves a PCC of 0.917 for horizon=2, outperforming the next best model, Epi-Cola-GNN, which scores 0.902. Among the other models, Epi-Cola-GNN and Epi-GNN show the second-best performances. While the forecasting accuracy of Epi-GNN is slightly inferior to HeatGNN in most tasks, it achieves the best performance in a few cases, highlighting its effectiveness and robustness in capturing spatio-temporal dependencies for epidemic forecasting.

As the forecasting horizon increases, HeatGNN maintains competitive performance, while several baseline models show significant error growth. Short-term forecasting performs well due to strong temporal dependencies, as evidenced by good forecasting performance for all models at horizon=2. However, traditional statistical and CNN-based models lose temporal dependency information as the horizon extends, leading to rapid performance declines. In contrast, the RNN-based models maintain relatively robust performance with their memory of temporal dependencies. The improved performance of STGNN models, such as Cola-GNN, STGCN, and TMGNN, highlights the importance of spatio-temporal heterogeneity in epidemic forecasting. Nevertheless, while spatio-temporal dependencies enhance the ability to capture dynamic changes in epidemic transmission, they also introduce added complexity, compromising the robustness of specific models, such as MGNN and ATMGNN. Additionally, incorporating epidemic mechanism models into GNNs improves short-term forecasting accuracy. For instance, Epi-Cola-GNN achieves the second-best performance across all three datasets at horizon=2.

F. Ablation Study

This section addresses **RQ2**. To assess the effect of each component in our framework, we conduct the ablation study by testing the following variants of HeatGNN:

- HeatGNN w/o PL: Remove the physics loss from HeatGNN removes the constraints on the EIEL module.
- HeatGNN w/o TG: Remove the TG module and use only the STGL module for direct forecasting, while retaining the EIEL module to guide the output of the framework.
- HeatGNN w/o TP: Remove the EIEL and TG modules and only keep the STGL module for forecasting.

The ablation study results of RMSE and PCC are shown in Table III. The results show that our proposed HeatGNN performs robustly across most cases, except for horizon=4 in the US-States dataset. The physical loss incorporates domain knowledge of epidemic transmission, particularly benefiting high-variability regions (e.g., Japan-Prefectures and US-Regions) and long-term forecasting. Removing the physics loss results in the model lacking intrinsic epidemic transmission mechanism constraints, which increases the forecasting error and reduces its ability to capture trends. However, its impact is limited in the US-States dataset, which is low volatility and relatively uniform data. The TG module is crucial for modeling cross-regional epidemic transmission. After removing the TG module, the model is significantly weaker at capturing the intrinsic epidemic transmission relationship between locations. While it has a similar role to the physics loss across datasets, its impact on forecasting performance is more pronounced. Additionally, the EIEL module enhances the effectiveness of the TG module, further improving the model’s ability to capture epidemic transmission. Relying solely on the STGL module is insufficient for addressing complex epidemic forecasting tasks. When both the TG and EIEL modules are removed, the model struggles to accurately capture epidemic transmission over extended time horizons, resulting in a significant decline in forecasting performance. These findings suggest that the modules interact synergistically to achieve optimal performance in HeatGNN.

G. Hyperparameter Sensitivity Analysis

This section addresses **RQ3**. We investigate how the forecasting performance varies with some hyperparameters.

1) *Window size*: To evaluate whether the model is sensitive to the length of historical data, we evaluate different window sizes ranging from 20 to 60. Figures 3 (a), (b), and (c) show the RMSE and PCC results in different window sizes. For the Japan-Prefectures dataset, forecasting performance improves significantly with larger window sizes, as evidenced by a gradual decrease in RMSE and an increase in PCC. This result suggests that a larger window size provides more comprehensive historical information, enhancing forecasting accuracy. In contrast, model performance remains stable across all window sizes for the US-Regions dataset, which indicates that the model is not sensitive to the window size change in this dataset. For the US-States dataset, the optimal performance

TABLE II: RMSE and PCC performance of different methods on three datasets with horizon = 2, 3, 4, 5. A boldface indicates the best result for each column, and the second-best is underlined.

RMSE(↓)	Japan-Prefectures				US-Regions				US-States			
	2	3	4	5	2	3	4	5	2	3	4	5
AR	1669.898	2071.535	2312.712	2440.119	625.620	813.453	956.083	1078.889	172.179	210.689	239.205	264.437
ARMA	1661.222	2070.781	2312.378	2438.737	622.393	804.126	939.212	1057.998	172.106	207.789	239.828	262.015
GAR	1484.372	1990.001	2281.875	2427.555	607.232	790.684	934.327	1053.783	161.848	199.566	220.901	247.398
VAR	1577.216	2100.213	2443.453	2566.043	694.516	864.829	1000.032	1112.857	297.669	306.723	318.044	333.312
RNN	1198.314	1551.096	1720.115	1851.500	572.438	753.568	890.801	979.708	158.949	195.903	210.525	224.040
LSTM	1255.470	1555.815	1710.241	1839.544	570.277	743.945	913.847	1048.754	161.029	197.831	216.700	226.667
GRU	1181.230	1498.437	1632.849	1781.807	570.898	741.786	893.440	1024.078	159.298	195.385	217.282	247.858
RNN-Attn	1311.157	1751.819	2056.583	2266.540	566.375	757.980	894.176	999.389	162.821	193.795	219.705	243.932
CNNRNN-Res	1401.394	1889.815	2260.501	2570.203	594.910	782.389	873.559	1006.251	228.275	290.916	308.268	320.370
LSTNet	1441.367	2030.374	2331.407	2385.490	606.540	841.441	1030.450	1134.228	195.949	232.584	255.764	276.306
STGCN	1273.563	1389.538	1498.233	1399.753	726.945	814.875	894.509	965.067	205.060	226.799	246.035	260.379
MGNN	1756.653	1922.766	1822.108	1943.240	1472.420	1415.071	1473.778	1487.338	178.034	189.710	198.840	205.517
TMGNN	1500.051	1471.865	1568.222	1558.965	656.364	755.206	829.295	915.758	178.709	188.653	201.361	190.089
ATMGNN	2436.255	2465.356	2473.451	2464.829	1553.142	1607.391	1691.877	1688.661	307.932	374.719	383.963	355.191
Cola-GNN	1167.715	1416.884	1478.782	1572.566	551.810	681.407	793.208	<u>870.818</u>	<u>147.700</u>	175.602	194.336	223.540
Epi-Cola-GNN	1118.387	2056.956	2282.738	1543.628	<u>546.637</u>	747.352	881.656	871.939	148.455	184.681	204.389	219.132
Epi-GNN	1503.244	<u>1296.059</u>	1284.933	1447.863	563.328	708.990	<u>790.972</u>	881.026	149.515	<u>168.939</u>	<u>184.500</u>	<u>190.005</u>
HeatGNN	<u>1148.850</u>	1260.150	<u>1295.697</u>	1378.207	540.573	<u>693.655</u>	781.513	852.311	142.433	164.788	177.624	186.280
PCC(↑)	2	3	4	5	2	3	4	5	2	3	4	5
AR	0.743	0.567	0.413	0.303	0.921	0.868	0.829	0.788	0.934	0.903	0.876	0.850
ARMA	0.745	0.567	0.413	0.303	0.920	0.870	0.827	0.786	0.933	0.902	0.873	0.849
GAR	0.803	0.613	0.444	0.318	0.924	0.870	0.823	0.782	0.938	0.906	0.884	0.861
VAR	0.771	0.564	0.369	0.229	0.895	0.839	0.775	0.715	0.779	0.769	0.749	0.730
RNN	0.887	0.810	0.775	0.757	0.934	0.886	0.848	0.819	0.944	0.915	0.902	0.890
LSTM	0.884	0.831	0.818	0.820	0.933	0.890	0.853	0.820	0.943	0.915	0.897	0.892
GRU	0.894	0.840	0.827	0.807	0.933	0.887	0.849	0.817	0.944	0.916	0.897	0.870
RNN-Attn	0.865	0.735	0.589	0.497	0.936	0.889	0.849	0.820	0.943	0.916	0.891	0.869
CNNRNN-Res	0.828	0.653	0.459	0.239	0.925	0.869	0.833	0.777	0.887	0.802	0.769	0.731
LSTNet	0.820	0.586	0.384	0.338	0.934	0.877	0.795	0.733	0.924	0.885	0.848	0.811
STGCN	0.892	0.874	0.852	<u>0.872</u>	0.899	0.866	0.848	0.831	0.901	0.882	0.861	0.838
MGNN	0.688	0.633	0.644	0.507	0.558	0.557	0.557	0.550	0.926	0.914	0.909	0.901
TMGNN	0.827	0.836	0.833	0.822	0.913	0.885	0.870	0.833	0.925	0.916	0.906	0.913
ATMGNN	0.160	0.156	0.162	0.170	0.496	0.481	0.464	0.456	0.737	0.640	0.633	0.698
Cola-GNN	0.906	0.845	0.870	0.834	0.939	0.903	0.872	0.847	<u>0.953</u>	0.936	0.922	0.904
Epi-Cola-GNN	<u>0.912</u>	0.580	0.444	0.859	<u>0.940</u>	0.889	0.851	<u>0.858</u>	<u>0.953</u>	0.922	0.906	0.909
Epi-GNN	0.821	0.911	0.911	0.869	0.937	<u>0.904</u>	<u>0.885</u>	<u>0.858</u>	0.952	<u>0.937</u>	<u>0.925</u>	0.923
HeatGNN	0.917	<u>0.907</u>	<u>0.910</u>	0.884	0.941	0.908	0.885	0.866	0.953	0.939	0.929	<u>0.921</u>

is observed at a window size of 60. In summary, while increasing the window size enhances model performance, the improvement becomes limited after a threshold.

2) *Horizon size*: To evaluate the sensitivity of the model to the size of the forecasting horizon, we analyze its performance across horizons ranging from 1 to 6. Figures 3 (d), (e), and (f) show the RMSE and PCC results for different horizons. In the Japan-Prefectures dataset, as the forecasting horizon increases, RMSE gradually rises while PCC decreases, indicating a decline in forecasting accuracy with longer horizons. Similar trends are observed in the US-Regions and US-States datasets. Comparing the results across the three datasets, we find that datasets with more significant fluctuations (Japan-Prefectures), shorter forecasting horizons, and more accurate predictions, while datasets with lower variability (US-Regions and US-States) maintain relatively robust forecasting performance even with longer horizons.

3) *Loss weight*: To evaluate the sensitivity of the model to the balance weight between physical and data loss, we examine the effect of varying λ values from 0 to 1 on forecasting performance. Figures 3 (g), (h), and (i) show the RMSE and PCC results under different λ . On the Japanese-Prefectures dataset, the PCC of the model remains stable as λ increases (i.e., the weight of the physical loss increases), while the RMSE increases slightly at $\lambda = 0.2$. This result indicates that performance is slightly affected by low physical loss weights, and the overall trend remains stable. Comparing the results across the three datasets, we observe that the Japan-Prefectures dataset performs slightly worse under low physical loss weights. In contrast, the US-States dataset performs best with higher physical loss weights. Overall, increasing the λ value has a greater impact on datasets with greater variability, while datasets with lower variability (e.g., US-States) maintain good performance even at higher λ values. These results suggest that reasonably adjusting the balance between physical

TABLE III: Ablation test results on three datasets.

RMSE(↓)	2	3	4	5
Japan-Prefectures				
HeatGNN w/o PL	1230.134	1360.714	1407.590	1453.051
HeatGNN w/o TG	1228.951	1331.692	1421.312	1438.525
HeatGNN w/o TP	1278.808	1322.376	1441.331	1451.568
HeatGNN	1148.850	1260.150	1295.697	1378.207
US-Regions				
HeatGNN w/o PL	631.080	799.733	869.248	942.947
HeatGNN w/o TG	739.933	811.149	854.826	1039.151
HeatGNN w/o TP	726.639	861.203	947.868	977.450
HeatGNN	540.573	693.655	781.513	852.311
US-States				
HeatGNN w/o PL	146.414	168.938	172.590	188.129
HeatGNN w/o TG	148.601	176.770	176.644	201.611
HeatGNN w/o TP	152.508	181.273	169.937	206.313
HeatGNN	142.433	164.788	177.624	186.280
PCC(↑)				
Japan-Prefectures				
HeatGNN w/o PL	0.900	0.889	0.876	0.863
HeatGNN w/o TG	0.891	0.895	0.898	0.871
HeatGNN w/o TP	0.890	0.893	0.893	0.853
HeatGNN	0.917	0.907	0.910	0.884
US-Regions				
HeatGNN w/o PL	0.924	0.892	0.875	0.864
HeatGNN w/o TG	0.923	0.891	0.881	0.838
HeatGNN w/o TP	0.927	0.895	0.866	0.854
HeatGNN	0.941	0.908	0.885	0.866
US-States				
HeatGNN w/o PL	0.951	0.933	0.929	0.917
HeatGNN w/o TG	0.951	0.927	0.930	0.907
HeatGNN w/o TP	0.951	0.925	0.932	0.902
HeatGNN	0.953	0.939	0.929	0.921

and data loss can enhance model performance across different datasets.

4) *Sparse Threshold*: To evaluate whether the model is sensitive to the sparsification of the MAG, we test the impact of different sparse thresholds, from 0 to 0.8 (Figures 3 (j), (k), and (l)). A higher threshold corresponds to a sparser MAG. On the Japan-Prefectures dataset, as the sparse threshold increases, RMSE fluctuates slightly, indicating that excessive sparsification may degrade the forecasting performance. On the US-Regions dataset, RMSE shows minor fluctuation, with mild sparsification improving model performance, while PCC remains stable, indicating that the model is not highly sensitive to changes in the sparse threshold. For the US-States dataset, the model achieves the best at a lower sparse threshold, with a slight decrease in PCC as the threshold increases. In summary, a modest increase in the sparse threshold can improve model performance, and selecting an appropriate threshold helps balance data complexity and model effectiveness.

H. Case Study

This section addresses **RQ4**. To demonstrate the effectiveness of the proposed HeatGNN in capturing spatio-temporal heterogeneity and mechanistic heterogeneity, we conduct a

case study to evaluate its short-term and long-term forecasting performance. Specifically, we select two locations from the Japan-Prefectures dataset. We analyze their forecasting performance under the short-term (horizon=2) and long-term (horizon=5) scenarios to explore the forecasting performance of the HeatGNN under different locations. In short-term forecasting (Figures 4(a) and 4(b)), the model accurately predicts the fluctuation trends of epidemic transmission risk. The model’s predictions are close to the actual situation both at the peak and trough of the epidemic, indicating that it is also applicable during extreme events (e.g., 8-10 weeks in Figure 4(a)). This peak sensitivity is critical in the epidemic response strategy, which helps to take interventions in advance to control outbreaks. The model performs stable prediction performance in long-term forecasting, in which the model captures the direction of risk fluctuations (Figures 4(c) and 4(d)). Furthermore, the model can predict a rapid rise in the epidemic 1-2 weeks before an outbreak in long-term forecasting, providing valuable lead time for early prevention efforts. To further validate our findings, we perform a similar analysis using data from the US-States dataset (Figure 5), and the results are consistent with those from the Japan-Prefectures dataset. Those results indicate that HeatGNN effectively captures both short-term and long-term epidemic transmission.

I. Inference Analysis

This section addresses **RQ5**. To verify the inference efficiency of our framework, we conduct an inference analysis experiment of different location scales based on the US-States dataset to evaluate the inference speed. The results in Figure 6 indicate that the inference time of the HeatGNN remains stable with only minor fluctuations under different location scales. This consistent performance demonstrates the robustness and reliability of HeatGNN, further highlighting its scalability and suitability for applications involving dynamic or large-scale epidemic transmission graph datasets.

V. RELATED WORK

A. Epidemic Forecasting

Epidemic forecasting is a critical task in monitoring the spread of epidemics to help public health interventions quickly and avoid large-scale outbreaks [36]. The time dependence and seasonality of epidemic spread are considered at the beginning of epidemic forecasting. Time series regression models, such as ARIMA [37] and VAR [38], and machine learning models, such as random forests [5], are widely used to solve this task, but these models cannot capture spatial dependencies and ignore the evolution of epidemic transmission. To further improve the ability of the model to capture temporal dependencies, the RNN and RNN-based models were proposed for this task [39]. CNN, Transformer, and their adopted models are used to capture multi-scale features, such as short-term temporal dependencies and long-term temporal dependencies [40]. Meanwhile, the emergence of GNN provides an effective solution to identifying spatio-temporal patterns in epidemic forecasting. In addition to most studies focusing on the impact

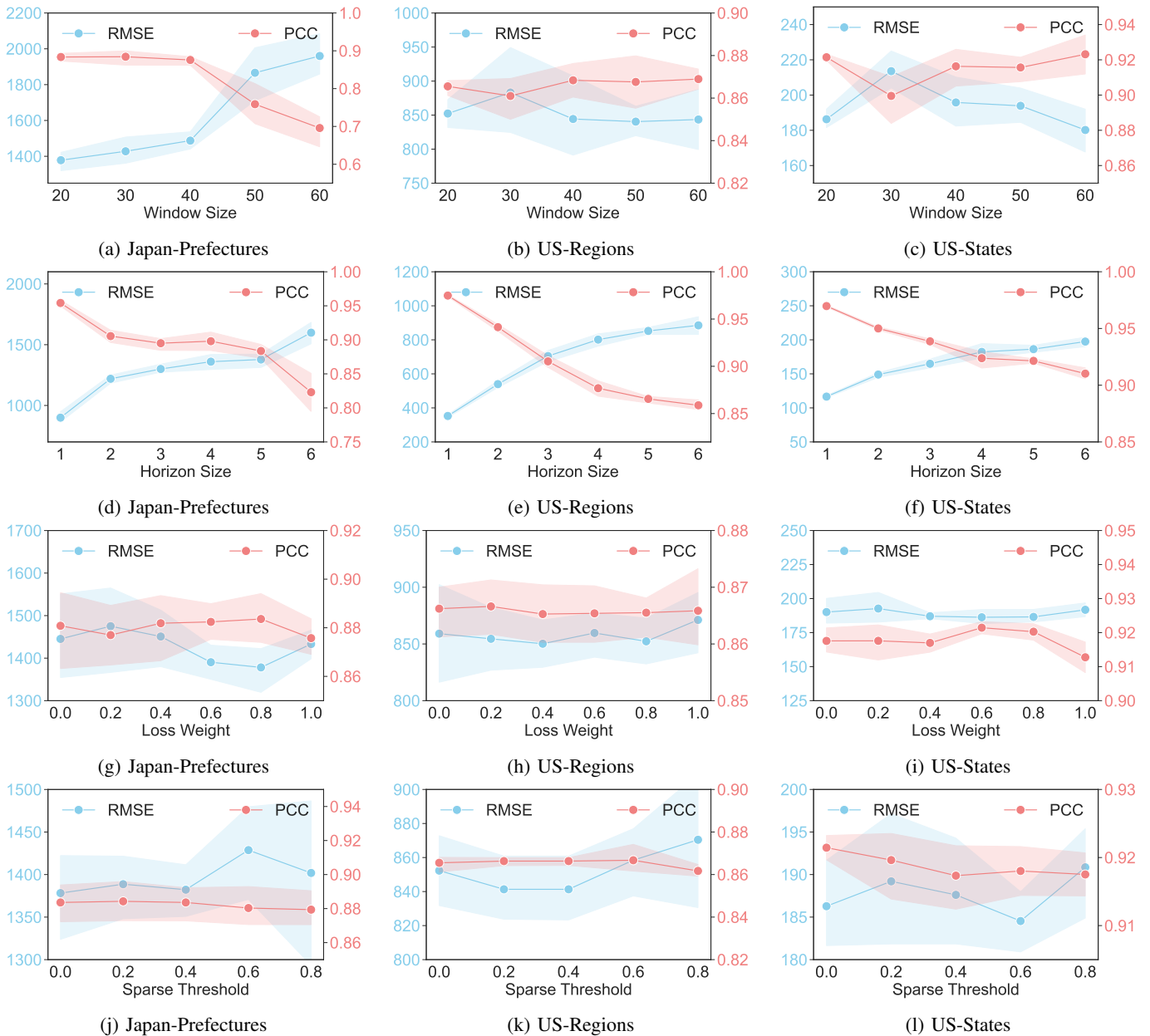
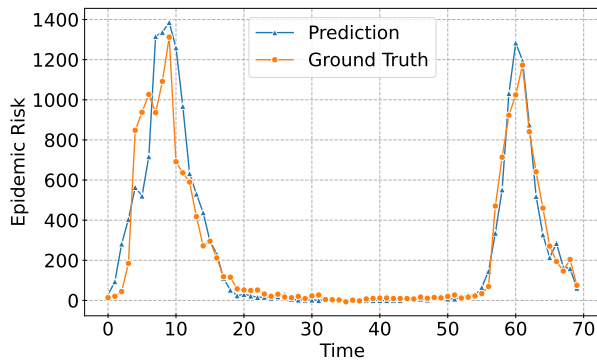


Fig. 3: Sensitivity analysis on hyperparameter in three real-world datasets. Performance with window size w , horizon size h , loss weight λ , and sparse threshold δ . The shaded area represents the 95% confidence interval. Except for the sensitivity analysis experiment of h , other sensitivity analysis experiments are conducted under horizon=5.

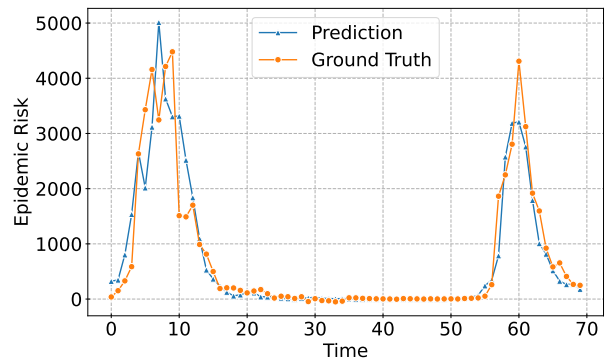
of geographic topology between locations [4], [12], [14], some studies focus on the distinction between local and global information in epidemic spread [12], as well as multi-scale information [13], [41]. However, these methods mainly focus on the spatio-temporal dependence of epidemic transmission but ignore intrinsic transmission patterns and the evolution of epidemics. They also lack mechanism models to describe the transmission mechanisms behind epidemics. These limitations make it challenging to provide sufficient information to support public health decision-making.

B. Spatio-temporal Graph Learning

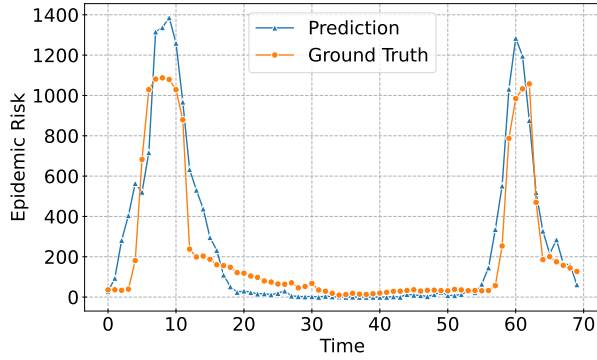
Recently, spatio-temporal graph learning has emerged as a powerful framework for modeling complex data structures that evolve over both spatial and temporal. Graph Convolutional Networks (GCNs) have been developed to achieve end-to-end learning of graph structures [42]. GCNs can efficiently capture local features by sharing parameters in the neighborhood of the graph. Since then, GNNs expanded from static graphs to dynamic graphs to handle the requirement of spatio-temporal data modeling from the needs of dynamic network tasks, like traffic [43], electric load [44], and epidemic [4] forecasting,



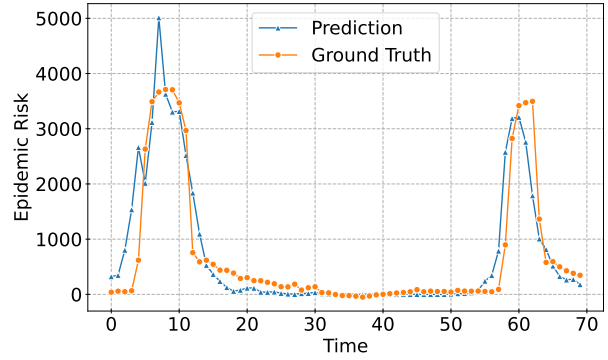
(a) No.0 Location



(b) No.25 Location

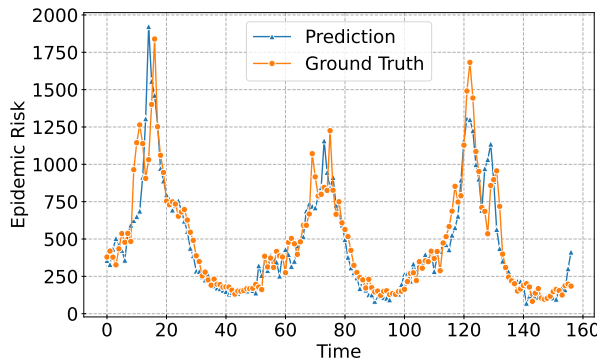


(c) No.0 Location

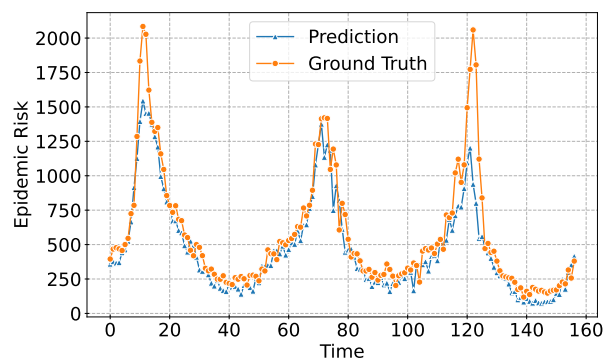


(d) No.25 Location

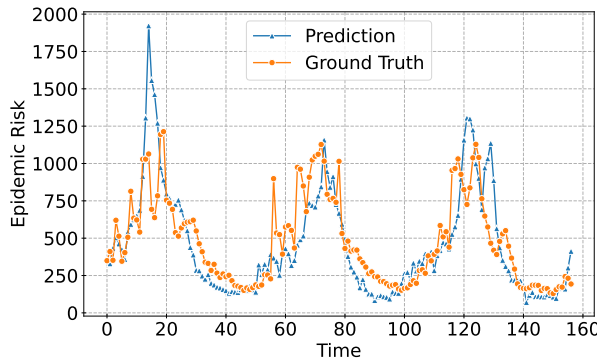
Fig. 4: Case study in Japan-Prefectures. (a) and (b) are conducted under horizon=2. (c) and (d) are conducted under horizon=5.



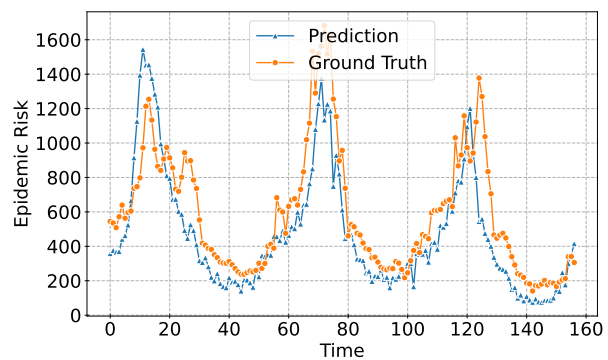
(a) No.0 Location



(b) No.7 Location



(c) No.0 Location



(d) No.7 Location

Fig. 5: Case study in US-Regions. (a) and (b) are conducted under horizon=2. (c) and (d) are conducted under horizon=5.

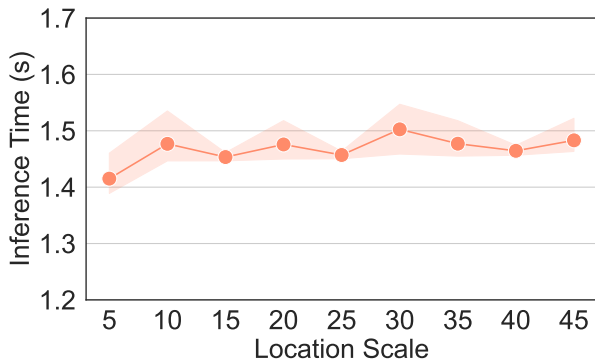


Fig. 6: Inference Analysis with different scale locations under horizon=5 in US-Regions.

which involves temporal evolution. The emergence of dynamic graph neural networks, like graph convolutional recurrent networks (GCRN), enables GNNs to update graph structures in time series and capture dynamic changes in node relationships [45]. To further integrate temporal and spatial dependencies, STGNNs combine graph convolution and temporal convolution, enabling the model to capture the dynamic characteristics of temporal and spatial simultaneously, showing significant advantages in various spatio-temporal data tasks [27].

With the development of spatio-temporal graph learning, some studies have introduced recurrent neural networks [46], [47] and Transformer-based attention mechanisms [48] to learn spatio-temporal dependencies more flexibly. In addition, the demand for spatio-temporal dependencies across different scales is driven by the proposed multiscale STGNNs [49]. STGNNs combined with the hypergraph structure are used to process complex high-order interactions in spatio-temporal graph learning [50], [51]. The spatio-temporal graph diffusion network was proposed to describe the information diffusion process in spatio-temporal graph learning [43]. Meanwhile, heterogeneous STGNNs have been proposed to better adapt to complex heterogeneity problems in spatio-temporal data [52]. Overall, STGNN can capture the spatio-temporal dependencies of epidemics well. Therefore, to enable our proposed framework to capture the spatio-temporal heterogeneity of various epidemic locations, we are inspired by [12] and use it as the spatio-temporal graph module.

C. Physics-guided Machine Learning

The approximations learned by machine learning methods often ignore or violate existing physical knowledge, leading to misleading or unexplainable conclusions [53]. Therefore, the combination of physics and machine learning has begun to be proposed to solve the problem of lack of interpretability and black-box structures in machine learning. A commonly used method is physics-informed neural networks (PINN) [28], which is based on combining physical residual loss with data loss to transfer or distill physical epidemic knowledge into a machine learning framework for constrained learning processes while being able to effectively capture heterogeneous data in different forecasting tasks, such as urban flow

[54], blood pressure [55], rumor detection [56], and epidemic transmission [19], [57]. Another way to combine physical models and machine learning is Neural differential equations (Neural ODEs), which use the neural network as a continuous dynamic process. For example, the time-dependent states in the epidemic model are replaced by neural networks [58]. Neural ODEs are also used in fields such as climate, weather [59], polar motion [60], and battery health [61] forecasting to solve real-world complex continuous-time systems.

Some scenarios in epidemic transmission require integrating physical models into machine learning models to improve performance and interpretability. Epidemic models are based on overly simple assumptions and cannot fully understand the complex epidemic spread [9], while machine learning models lack effective mechanism explanations. Extended epidemic models with networks have been proposed to describe the transmission patterns between locations [11], [62]. However, these network-based epidemic models have problems with large-scale parameter optimization [11] or lack of data [21], [63]. To address those problems, some models proposed to use simulated data generated by physical models to solve the problem of insufficient data and provide high-resolution forecasting [17], [63]. Meanwhile, machine learning has also begun to estimate epidemic models to solve the parameter explosion [20], [21]. Neural ODEs are incorporated into epidemic models to learn the continuous evolution of epidemic spread in different regions [18]. The epidemic models were used as causal mechanism models to guide the graph embedding learning process to handle noisy data and missing data better [64]. Although physics-guided machine learning has made efforts in epidemic forecasting, previous studies have ignored the mutual influence and dependency of the intrinsic epidemic transmission between locations, which makes it challenging to forecast epidemics breaking out in multiple locations.

VI. CONCLUSION

In this study, we propose a novel epidemic forecasting framework, HeatGNN, to improve the forecasting performance. We incorporate the epidemic mechanism model into the epidemiology-informed embedding learning to learn intrinsic epidemic transmission patterns. We use the physics loss to constrain the epidemiology-informed location embeddings to align with real-world epidemics. We propose a mechanistic affinity graph to represent the mechanistic dependence of intrinsic epidemic transmission between locations. We design a heterogeneous transmission graph network to account for the mechanistic heterogeneity. Finally, the forecasting performance is further improved by combining the spatio-temporal graph learning and transmission graph modules. The effectiveness of HeatGNN is validated using real-world datasets for epidemic forecasting. Experimental results demonstrate that HeatGNN is capable of outperforming existing state-of-the-art models in epidemic forecasting. In the future, we plan to construct an interpretable mechanistic affinity graph with mechanisms models to cope with the spatio-temporal and mechanistic heterogeneity.

REFERENCES

- [1] A. D. Proal and M. B. VanElzakker, "Long covid or post-acute sequelae of covid-19 (pasc): an overview of biological factors that may contribute to persistent symptoms," *Frontiers in microbiology*, vol. 12, p. 698169, 2021.
- [2] M. Lenzen, M. Li, A. Malik, F. Pomponi, Y.-Y. Sun, T. Wiedmann, F. Faturay, J. Fry, B. Gallejo, A. Geschke *et al.*, "Global socio-economic losses and environmental gains from the coronavirus pandemic," *PLoS one*, vol. 15, no. 7, p. e0235654, 2020.
- [3] S. P. Adhikari, S. Meng, Y.-J. Wu, Y.-P. Mao, R.-X. Ye, Q.-Z. Wang, C. Sun, S. Sylvia, S. Rozelle, H. Raat *et al.*, "Epidemiology, causes, clinical manifestation and diagnosis, prevention and control of coronavirus disease (covid-19) during the early outbreak period: a scoping review," *Infectious diseases of poverty*, vol. 9, pp. 1–12, 2020.
- [4] S. Deng, S. Wang, H. Rangwala, L. Wang, and Y. Ning, "Cola-gnn: Cross-location attention based graph neural networks for long-term ili prediction," in *Proceedings of the 29th ACM international conference on information & knowledge management*, 2020, pp. 245–254.
- [5] C. Zhan, Y. Zheng, H. Zhang, and Q. Wen, "Random-forest-bagging broad learning system with applications for covid-19 pandemic," *IEEE Internet of Things Journal*, vol. 8, no. 21, pp. 15906–15918, 2021.
- [6] C. Zhan, Y. Zheng, L. Shao, G. Chen, and H. Zhang, "Modeling the spread dynamics of multiple-variant coronavirus disease under public health interventions: A general framework," *Information Sciences*, vol. 628, pp. 469–487, 2023.
- [7] Z.-Y. Chen, M. Sun, and X.-X. Han, "Prediction-driven collaborative emergency medical resource allocation with deep learning and optimization," *Journal of the Operational Research Society*, vol. 74, no. 2, pp. 590–603, 2023.
- [8] S. Saha, G. Samanta, and J. J. Nieto, "Epidemic model of covid-19 outbreak by inducing behavioural response in population," *Nonlinear dynamics*, vol. 102, pp. 455–487, 2020.
- [9] W. O. Kermack and A. G. McKendrick, "A contribution to the mathematical theory of epidemics," *Proceedings of the royal society of london. Series A, Containing papers of a mathematical and physical character*, vol. 115, no. 772, pp. 700–721, 1927.
- [10] E. L. Campos, R. P. Cysne, A. L. Madureira, and G. L. Mendes, "Multi-generational sir modeling: Determination of parameters, epidemiological forecasting and age-dependent vaccination policies," *Infectious Disease Modelling*, vol. 6, pp. 751–765, 2021.
- [11] C. Zhan, Y. Zheng, Z. Lai, T. Hao, and B. Li, "Identifying epidemic spreading dynamics of covid-19 by pseudoco-evolutionary simulated annealing optimizers," *Neural Computing and Applications*, vol. 33, pp. 4915–4928, 2021.
- [12] F. Xie, Z. Zhang, L. Li, B. Zhou, and Y. Tan, "Epi-gnn: Exploring spatial transmission with graph neural network for regional epidemic forecasting," in *Joint European Conference on Machine Learning and Knowledge Discovery in Databases*. Springer, 2022, pp. 469–485.
- [13] M. Qiu, Z. Tan, and B.-k. Bao, "Msgnn: Multi-scale spatio-temporal graph neural network for epidemic forecasting," *Data Mining and Knowledge Discovery*, pp. 1–29, 2024.
- [14] G. Panagopoulos, G. Nikolentzos, and M. Vazirgiannis, "Transfer graph neural networks for pandemic forecasting," in *Proceedings of the AAAI Conference on Artificial Intelligence*, vol. 35, no. 6, 2021, pp. 4838–4845.
- [15] T. S. Hy, V. B. Nguyen, L. Tran-Thanh, and R. Kondor, "Temporal multiresolution graph neural networks for epidemic prediction," in *Workshop on Healthcare AI and COVID-19*. PMLR, 2022, pp. 21–32.
- [16] V. B. Nguyen, T. S. Hy, L. Tran-Thanh, and N. Nghiem, "Predicting covid-19 pandemic by spatio-temporal graph neural networks: A new zealand's study," *arXiv preprint arXiv:2305.07731*, 2023.
- [17] L. Wang, J. Chen, and M. Marathe, "Defsi: Deep learning based epidemic forecasting with synthetic information," in *Proceedings of the AAAI conference on artificial intelligence*, vol. 33, no. 01, 2019, pp. 9607–9612.
- [18] G. Wan, Z. Liu, M. S. Lau, B. A. Prakash, and W. Jin, "Epidemiology-aware neural ode with continuous disease transmission graph," *arXiv preprint arXiv:2410.00049*, 2024.
- [19] A. Rodríguez, J. Cui, N. Ramakrishnan, B. Adhikari, and B. A. Prakash, "Einns: epidemiologically-informed neural networks," in *Proceedings of the AAAI conference on artificial intelligence*, vol. 37, no. 12, 2023, pp. 14453–14460.
- [20] M. Liu, Y. Liu, and J. Liu, "Epidemiology-aware deep learning for infectious disease dynamics prediction," in *Proceedings of the 32nd ACM International Conference on Information and Knowledge Management*, 2023, pp. 4084–4088.
- [21] Q. Cao, R. Jiang, C. Yang, Z. Fan, X. Song, and R. Shibasaki, "Mepognn: Metapopulation epidemic forecasting with graph neural networks," in *Joint European Conference on Machine Learning and Knowledge Discovery in Databases*. Springer, 2022, pp. 453–468.
- [22] I. F. Miller, A. D. Becker, B. T. Grenfell, and C. J. E. Metcalf, "Disease and healthcare burden of covid-19 in the united states," *Nature medicine*, vol. 26, no. 8, pp. 1212–1217, 2020.
- [23] X. Liu, J. Huang, C. Li, Y. Zhao, D. Wang, Z. Huang, and K. Yang, "The role of seasonality in the spread of covid-19 pandemic," *Environmental research*, vol. 195, p. 110874, 2021.
- [24] N. G. Davies, P. Klepac, Y. Liu, K. Prem, M. Jit, and R. M. Eggo, "Age-dependent effects in the transmission and control of covid-19 epidemics," *Nature medicine*, vol. 26, no. 8, pp. 1205–1211, 2020.
- [25] K. O. Kwok, F. Lai, W. I. Wei, S. Y. S. Wong, and J. W. Tang, "Herd immunity—estimating the level required to halt the covid-19 epidemics in affected countries," *Journal of Infection*, vol. 80, no. 6, pp. e32–e33, 2020.
- [26] H. Gibbs, Y. Liu, C. A. Pearson, C. I. Jarvis, C. Grundy, B. J. Quilty, C. Diamond, and R. M. Eggo, "Changing travel patterns in china during the early stages of the covid-19 pandemic," *Nature communications*, vol. 11, no. 1, p. 5012, 2020.
- [27] B. Yu, H. Yin, and Z. Zhu, "Spatio-temporal graph convolutional networks: A deep learning framework for traffic forecasting," *arXiv preprint arXiv:1709.04875*, 2017.
- [28] M. Raissi, P. Perdikaris, and G. E. Karniadakis, "Physics informed deep learning (part i): Data-driven solutions of nonlinear partial differential equations," *arXiv preprint arXiv:1711.10561*, 2017.
- [29] Y. Wu, Y. Yang, H. Nishiura, and M. Saitoh, "Deep learning for epidemiological predictions," in *The 41st international ACM SIGIR conference on research & development in information retrieval*, 2018, pp. 1085–1088.
- [30] D. P. Kingma, "Adam: A method for stochastic optimization," *arXiv preprint arXiv:1412.6980*, 2014.
- [31] P. J. Werbos, "Backpropagation through time: what it does and how to do it," *Proceedings of the IEEE*, vol. 78, no. 10, pp. 1550–1560, 1990.
- [32] A. Graves and A. Graves, "Long short-term memory," *Supervised sequence labelling with recurrent neural networks*, pp. 37–45, 2012.
- [33] R. Dey and F. M. Salem, "Gate-variants of gated recurrent unit (gru) neural networks," in *2017 IEEE 60th international midwest symposium on circuits and systems (MWSCAS)*. IEEE, 2017, pp. 1597–1600.
- [34] J. Cheng, "Long short-term memory-networks for machine reading," *arXiv preprint arXiv:1601.06733*, 2016.
- [35] G. Lai, W.-C. Chang, Y. Yang, and H. Liu, "Modeling long-and short-term temporal patterns with deep neural networks," in *The 41st international ACM SIGIR conference on research & development in information retrieval*, 2018, pp. 95–104.
- [36] Z. Liu, G. Wan, B. A. Prakash, M. S. Lau, and W. Jin, "A review of graph neural networks in epidemic modeling," in *Proceedings of the 30th ACM SIGKDD Conference on Knowledge Discovery and Data Mining*, 2024, pp. 6577–6587.
- [37] D. Benvenuto, M. Giovanetti, L. Vassallo, S. Angeletti, and M. Ciccozzi, "Application of the arima model on the covid-2019 epidemic dataset," *Data in brief*, vol. 29, p. 105340, 2020.
- [38] A. C. Shang, K. E. Galow, and G. G. Galow, "Regional forecasting of covid-19 caseload by non-parametric regression: a var epidemiological model," *AIMS public health*, vol. 8, no. 1, p. 124, 2021.
- [39] P. Wang, X. Zheng, G. Ai, D. Liu, and B. Zhu, "Time series prediction for the epidemic trends of covid-19 using the improved lstm deep learning method: Case studies in russia, peru and iran," *Chaos, Solitons & Fractals*, vol. 140, p. 110214, 2020.
- [40] N. Wu, B. Green, X. Ben, and S. O'Banion, "Deep transformer models for time series forecasting: The influenza prevalence case," *arXiv preprint arXiv:2001.08317*, 2020.
- [41] Y. Tang, H. Wang, and Y. Li, "Enhancing spatial spread prediction of infectious diseases through integrating multi-scale human mobility dynamics," in *Proceedings of the 31st ACM International Conference on Advances in Geographic Information Systems*, 2023, pp. 1–12.
- [42] T. N. Kipf and M. Welling, "Semi-supervised classification with graph convolutional networks," *arXiv preprint arXiv:1609.02907*, 2016.

- [43] X. Zhang, C. Huang, Y. Xu, L. Xia, P. Dai, L. Bo, J. Zhang, and Y. Zheng, "Traffic flow forecasting with spatial-temporal graph diffusion network," in *Proceedings of the AAAI conference on artificial intelligence*, vol. 35, no. 17, 2021, pp. 15 008–15 015.
- [44] W. Lin and D. W. 0044, "Residential electric load forecasting via attentive transfer of graph neural networks." in *IJCAI*, 2021, pp. 2716–2722.
- [45] Y. Seo, M. Defferrard, P. Vandergheynst, and X. Bresson, "Structured sequence modeling with graph convolutional recurrent networks," in *Neural Information Processing: 25th International Conference, ICONIP 2018, Siem Reap, Cambodia, December 13-16, 2018, Proceedings, Part I 25*. Springer, 2018, pp. 362–373.
- [46] Y. Li, R. Yu, C. Shahabi, and Y. Liu, "Diffusion convolutional recurrent neural network: Data-driven traffic forecasting," *arXiv preprint arXiv:1707.01926*, 2017.
- [47] A. Cini, I. Marisca, F. M. Bianchi, and C. Alippi, "Scalable spatiotemporal graph neural networks," in *Proceedings of the AAAI conference on artificial intelligence*, vol. 37, no. 6, 2023, pp. 7218–7226.
- [48] R. Zha, L. Zhang, S. Li, J. Zhou, T. Xu, H. Xiong, and E. Chen, "Scaling up multivariate time series pre-training with decoupled spatial-temporal representations," in *2024 IEEE 40th International Conference on Data Engineering (ICDE)*. IEEE, 2024, pp. 667–678.
- [49] M. Li, S. Chen, Y. Zhao, Y. Zhang, Y. Wang, and Q. Tian, "Multiscale spatio-temporal graph neural networks for 3d skeleton-based motion prediction," *IEEE Transactions on Image Processing*, vol. 30, pp. 7760–7775, 2021.
- [50] Y. Zhao, X. Luo, W. Ju, C. Chen, X.-S. Hua, and M. Zhang, "Dynamic hypergraph structure learning for traffic flow forecasting," in *2023 IEEE 39th International Conference on Data Engineering (ICDE)*. IEEE, 2023, pp. 2303–2316.
- [51] Z. Li, C. Huang, L. Xia, Y. Xu, and J. Pei, "Spatial-temporal hypergraph self-supervised learning for crime prediction," in *2022 IEEE 38th international conference on data engineering (ICDE)*. IEEE, 2022, pp. 2984–2996.
- [52] C. Song, Y. Lin, S. Guo, and H. Wan, "Spatial-temporal synchronous graph convolutional networks: A new framework for spatial-temporal network data forecasting," in *Proceedings of the AAAI conference on artificial intelligence*, vol. 34, no. 01, 2020, pp. 914–921.
- [53] Y. Wu, B. Sicard, and S. A. Gadsden, "Physics-informed machine learning: A comprehensive review on applications in anomaly detection and condition monitoring," *Expert Systems with Applications*, p. 124678, 2024.
- [54] W. Jiang, T. Chen, G. Ye, W. Zhang, L. Cui, Z. Huang, and H. Yin, "Physics-guided active sample reweighting for urban flow prediction," in *Proceedings of the 33rd ACM International Conference on Information and Knowledge Management*, 2024, pp. 1004–1014.
- [55] K. Sel, A. Mohammadi, R. I. Pettigrew, and R. Jafari, "Physics-informed neural networks for modeling physiological time series for cuffless blood pressure estimation," *npj Digital Medicine*, vol. 6, no. 1, p. 110, 2023.
- [56] W. Jiang, T. Chen, X. Gao, W. Zhang, L. Cui, and H. Yin, "Epidemiology-informed network for robust rumor detection," *arXiv preprint arXiv:2411.12949*, 2024.
- [57] D. Wang, S. Zhang, and L. Wang, "Deep epidemiological modeling by black-box knowledge distillation: an accurate deep learning model for covid-19," in *Proceedings of the AAAI Conference on Artificial Intelligence*, vol. 35, no. 17, 2021, pp. 15 424–15 430.
- [58] C. Kosma, G. Nikolentzos, G. Panagopoulos, J.-M. Steyaert, and M. Vazirgiannis, "Neural ordinary differential equations for modeling epidemic spreading," *Transactions on Machine Learning Research*, 2023.
- [59] Y. Verma, M. Heinonen, and V. Garg, "Climode: Climate and weather forecasting with physics-informed neural odes," *arXiv preprint arXiv:2404.10024*, 2024.
- [60] M. Kiani Shahvandi, M. Schartner, and B. Soja, "Neural ode differential learning and its application in polar motion prediction," *Journal of Geophysical Research: Solid Earth*, vol. 127, no. 11, p. e2022JB024775, 2022.
- [61] S. Pepe, J. Liu, E. Quattrocchi, and F. Ciucci, "Neural ordinary differential equations and recurrent neural networks for predicting the state of health of batteries," *Journal of Energy Storage*, vol. 50, p. 104209, 2022.
- [62] A. Desiderio, G. Salina, and G. Cimini, "Multiplex mobility network and metapopulation epidemic simulations of italy based on open data," *Journal of Physics: Complexity*, vol. 3, no. 4, p. 04LT01, 2022.
- [63] J. Gao, J. Heintz, C. Mack, L. Glass, A. Cross, and J. Sun, "Evidence-driven spatiotemporal covid-19 hospitalization prediction with ising dynamics," *Nature communications*, vol. 14, no. 1, p. 3093, 2023.
- [64] L. Wang, A. Adiga, J. Chen, A. Sadilek, S. Venkatramanan, and M. Marathe, "Causalgnn: Causal-based graph neural networks for spatio-temporal epidemic forecasting," in *Proceedings of the AAAI conference on artificial intelligence*, vol. 36, no. 11, 2022, pp. 12 191–12 199.